# Adaptation to steady light by intrinsically photosensitive retinal ganglion cells

Michael Tri Hoang Do[1,2] and King-Wai Yau[2]

Solomon H. Snyder Department of Neuroscience and Center for Sensory Biology, The Johns Hopkins University School of Medicine, Baltimore, MD 21205

Contributed by King-Wai Yau, March 18, 2013 (sent for review December 16, 2012)

**Intrinsically photosensitive retinal ganglion cells (ipRGCs) are recently discovered photoreceptors in the mammalian eye. These photoreceptors mediate primarily nonimage visual functions, such as pupillary light reflex and circadian photoentrainment, which are generally expected to respond to the absolute light intensity. The classical rod and cone photoreceptors, on the other hand, mediate image vision by signaling contrast, accomplished by adaptation to light. Experiments by others have indicated that the ipRGCs do, in fact, light-adapt. We found the same but, in addition, have now quantified this light adaptation for the M1 ipRGC subtype. Interestingly, in incremental-flash-on-background experiments, the ipRGC's receptor current showed a flash sensitivity that adapted in background light according to the Weber–Fechner relation, well known to describe the adaptation behavior of rods and cones. Part of this light adaptation by ipRGCs appeared to be triggered by a $Ca^{2+}$ influx, in that the flash response elicited in the absence of extracellular $Ca^{2+}$ showed a normal rising phase but a slower decay phase, resulting in longer time to peak and higher sensitivity. There is, additionally, a prominent $Ca^{2+}$-independent component of light adaptation not typically seen in rods and cones or in invertebrate rhabdomeric photoreceptors.**

mammal | melanopsin | phototransduction | gain control

It has become clear over the past decade that the mammalian retina contains another photoreceptor class besides rods and cones, consisting of a subpopulation of retinal ganglion cells (RGCs) that are intrinsically photosensitive (ipRGCs) by virtue of their expression of the visual pigment, melanopsin (1–7). In mouse, these cells have been distinguished into subtypes: M1 through M5 (4–7). The first three can be visualized immunocytochemically with antibodies against melanopsin (with the M1 cells showing a higher melanopsin level than the other two) and have distinct morphological and physiological properties (4–14). M4 and M5 cells cannot be labeled by conventional immunocytochemistry, presumably because they have too little melanopsin, and are generally visualized more indirectly (12) [most recently, however, M4 cells have been revealed by immunofluorescence after signal amplification (15)]. The different subtypes also have somewhat distinct projection targets in the brain, mostly for nonimage visual functions (12, 14, 16, 17), with two prominent ones being the suprachiasmatic nucleus (master circadian pacemaker) and the olivary pretectal nucleus (control center for pupillary constriction) (12, 14–17). IpRGCs also innervate image-vision centers in the brain, such as the superior colliculus and the dorsal lateral geniculate nucleus, with the degree of innervation varying across subtypes (12, 15–19).

Because of the prominent roles played by ipRGCs in nonimage visual functions, such as those given above, a question has been whether these photoreceptors adapt to light. In principle, strict photon counting may be sufficient for fulfilling nonimage functions, although some light adaptation would be beneficial for extending the operating range of the cells with respect to light intensity. Rods and cones, on the other hand, are quite different. Their primary role in image vision, with one key aspect being the detection of contrast, practically necessitates adaptation to light. In fact, the well-known Weber–Fechner behavior of light adaptation by rods and cones (20) promotes constancy in object appearance regardless of the ambient irradiance, a highly desirable property for image vision (21). Accordingly, besides whether ipRGCs adapt to light, another question is, if they do adapt, whether their adaptation behavior resembles that shown by rods and cones (20). Previous work by others has indicated that these ganglion-cell photoreceptors indeed adapt (8, 22, 23), but these experiments were largely qualitative. We report here quantitative measurements of this adaptation. At the same time, we have taken a step toward understanding the mechanisms underlying adaptation. Our experiments focused on M1 ipRGCs, which offer the advantage of having much higher photosensitivity and much larger light responses than the other subtypes, thus permitting more precise measurements.

## Results

**Response of IpRGCs to Steady Light.** We made perforated-patch, voltage-clamp recordings (−80 mV; at 23 °C for cell stability) from ipRGCs identified based on their fluorescence in the flat-mount retina of the *Opn4:tdTomato* BAC transgenic mouse line (24) (*Materials and Methods*). We focused on ipRGCs with small somata, strong fluorescence, and large saturated photocurrents (generally >300 pA), likely the M1 subtype (8, 10, 12, 15). This subtype also has a much higher intrinsic photosensitivity than the others (8, 10, 12, 15) and is the major RGC subtype projecting to the suprachiasmatic nucleus for circadian photoentrainment (6, 12, 14, 17). In all recordings, synaptic transmission from the rod and cone pathways was blocked pharmacologically to isolate the intrinsic light response (24) (*Materials and Methods*).

When stimulated with a dim, long step of light (1–3 min; 40- to 730-μm light spot centered on the soma; *Materials and Methods*), the ipRGC exhibited a photocurrent that increased slowly to a steady level (Fig. 1*A*, top trace, and Fig. S1). Brighter steps elicited an increasingly faster and larger photocurrent but also an increasingly pronounced relaxation of the current from a transient peak, which is a sign of light adaptation. For the brightest steps, the photocurrent fell nearly to baseline before rising slowly again to a steady level equal to just a few percent of the transient peak in amplitude (Fig. 1*A*, bottom two traces; experiment with longer light step shown in Fig. 1*B*; 15 cells). Upon light off, the response decayed exponentially, with a time constant of ∼20 s for the weakest responses (with current <10 pA for a large light spot) and of ∼1 s for near-saturated responses (with transient-peak current generally >300 pA for a large light spot). Full recovery of dim-flash sensitivity required 1–2 min after the dimmest steps and >15 min after the brightest steps (nine cells); in other words, the recovery from adaptation is far slower than the response

Author contributions: M.T.H.D. and K.-W.Y. designed research; M.T.H.D. performed research; M.T.H.D. and K.-W.Y. analyzed data; and M.T.H.D. and K.-W.Y. wrote the paper.

The authors declare no conflict of interest.

[1]Present address: F. M. Kirby Neurobiology Center and Department of Neurology, Boston Children's Hospital and Harvard Medical School, Boston, MA 02115.

[2]To whom correspondence may be addressed. E-mail: michael.do@childrens.harvard.edu or kwyau@mail.jhmi.edu.

This article contains supporting information online at www.pnas.org/lookup/suppl/doi:10.1073/pnas.1304039110/-/DCSupplemental.

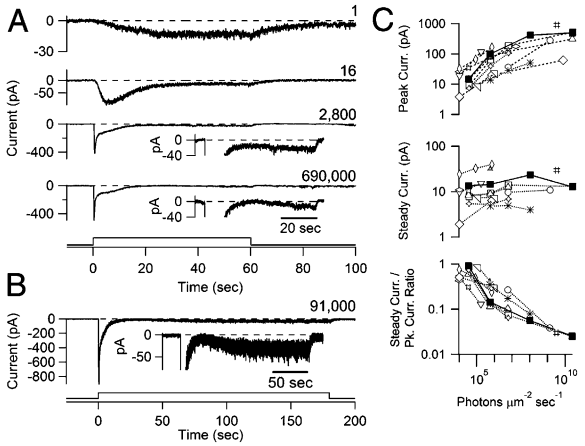


**Fig. 1.** Responses of ipRGCs to long steps of light. Perforated-patch, voltage-clamp recordings (–80 mV) of ipRGCs were obtained in flat-mount retina at 23 °C. (*A*) Responses of a cell to 1-min steps of diffuse light, increasing in intensity from top to bottom: $3.5 \times 10^4$, $5.7 \times 10^5$, $1.0 \times 10^8$, and $2.4 \times 10^{10}$ photons per square micron per second; light was at 480 nm except for the brightest, which was white but expressed as equivalent 480-nm photons. Relative light intensity is indicated on the right of each trace. Note the different scalings of ordinates. *Insets* are the same traces plotted on an expanded ordinate and contracted time scale. (*B*) Response of a different cell to a 3-min step of white light equivalent to $3.2 \times 10^9$ photons per square micron per second of 480-nm light (250-μm spot centered on soma). (*B*, *Inset*) Expanded ordinate and contracted time scale to show a transient, nearly complete loss of photocurrent attributable to adaptation, followed by a slow rise to steady plateau. (*C*) Properties of step responses plotted (for 15 cells) against light intensity, consisting of the peak current attained during the step, the steady current at the end of the step, and the ratio of the two. Each cell is denoted by a different symbol, with filled symbols corresponding to the cell in *A*. The steady currents at the highest intensity are likely to be somewhat smaller than true steady state, owing to their not having reached plateau at the time of measurement. Dispersion in the data are likely attributable to variation in sensitivity among cells and in the spot size used for stimulation. Light monitors are shown at the bottom of *A* and *B*. Ames medium with blockers of fast-synaptic transmission was used (*Materials and Methods*).

decay. Overall, brighter lights produced larger peak currents and typically also (slightly) larger steady currents, but the steady current was a progressively smaller fraction of the peak current (Fig. 1*C*). We observed a similar adaptation in acutely dissociated cells.

**Adaptation Behavior of IpRGCs to Steady Light.** To quantify light adaptation, we adopted a protocol used routinely for rods and cones, namely, measuring an ipRGC's receptor-current response to a dim test flash [i.e., driving the cell within its linear range (24)] superimposed on different background lights (20). The flash sensitivity, $S_F$, defined as dim-flash-response amplitude divided by flash intensity (25, 26), decreased progressively with increasing background intensity, $I_B$. Defined as such, $S_F$ embodies the combined effects of active and passive adaptations (20), with one component of the latter reflecting simply a sublinear increase (compression) of the light response as it gradually approaches saturation (20). For rods, compression is substantial because their limited active adaptation produces only a moderate relaxation of their light-step response (27). For cones, the more severe relaxation of their light-step response means that compression has a lesser role in light adaptation (27). As for ipRGCs, their steady-light response is even smaller than that of cones (Fig. 1), so the effect of compression is practically negligible. Nonetheless, ipRGCs showed a relation between log $S_F$ and log $I_B$ that agreed remarkably well with the well-known Weber–Fechner relation found for rods and cones (20), namely, $S_F \propto 1/[1 + (I_B/I_O)]$ (Fig. 2*A*, plotted in normalized units, i.e., $S_F/S_F{}^D$ against $I_B/I_O$, where $S_F{}^D$ is the flash sensitivity with no background light, and $I_O$ is the background intensity that reduced the cell's dark-adapted flash sensitivity by half; see also Fig. S2 *A–D*). The limited brightness of our light source did not allow interrogation of $S_F/S_F{}^D$ below ~$10^{-3}$. $I_O$ ranged from $1.2 \times 10^4$ to $2.7 \times 10^5$ photons (480 nm) per square micron per second (mean ± SD = $1.1 \pm 1.3 \times 10^5$ photons per square micron per second; $n = 5$ cells). This somewhat large spread in $I_O$ is similar to the spread in sensitivity previously observed for these cells (8, 24, 28). Although all recorded cells, based on their large saturated photocurrents (see above), apparently belonged to the M1 subtype, this subtype does display some molecular heterogeneity (13, 29), thus potentially some subtle variation in electrophysiological properties as well. The average $I_O$ is similar to that for primate cones (30) (Fig. S2*E*) when expressed in incident photons per square micron per second at the respective $\lambda_{max}$ but is very different in terms of the actual number of pigment molecules activated: $I_O$ is of the order of a few activated melanopsin molecules per second for the ipRGCs here (*SI Text*) and $2.6 \times 10^4$ $s^{-1}$ for cones (30). IpRGCs absorb relatively few photons, but their exceedingly slow responses integrate strongly with time (24), whereas cones absorb many more photons, but their fast responses integrate little (30, 31).

In addition to reducing flash sensitivity, background light shortened the time course of the ipRGC's flash response, primarily by accelerating the response termination, as also found in rods and cones (20, 31) (Fig. 2*B*). Because the response's rising phase changed little, the accelerated response termination intruded much sooner into the rising phase, consequently decreasing the response time to peak (Fig. 2*B*, *Lower*, with all response amplitudes normalized to the same height) and reducing the response amplitude (hence sensitivity; Fig. 2*B*, *Upper*). The duration of the dim-flash response can be described by its integration time, $t_i = \int f(t)dt/f_p$, where $f(t)$ is the dim-flash-response profile, and $f_p$ is its transient-peak amplitude (20). When normalized $t_i$ (i.e., $t_i/t_i{}^D$, where $t_i{}^D$ is

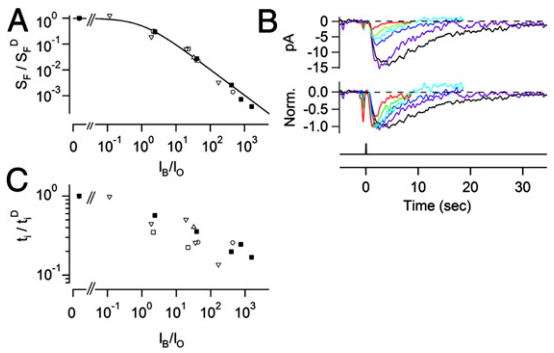


**Fig. 2.** Parameters of ipRGC adaptation. (*A*) Normalized flash sensitivity ($S_F/S_F{}^D$; *Results*) plotted against normalized background-light intensity ($I_B/I_O$; *Results*). Fit (solid black line) is the Weber–Fechner relation, $S_F/S_F{}^D = 1/[1 + (I_B/I_O)]$ (*Results*). Test flashes (50 ms) and steady backgrounds were diffuse, dim 480-nm light. Different symbols correspond to different cells, with filled black squares corresponding to the cell in *B*. All cells have the same data point at $S_F/S_F{}^D = 1$ and $I_B/I_O = 0$. (*B*, *Upper*) Flash responses from one cell, elicited in the presence of progressively brighter background lights (flashes from $1.2 \times 10^5$ to $5.4 \times 10^7$ photons per square micron and backgrounds from $3.1 \times 10^4$ to $2.0 \times 10^7$ photons per square micron per second; warmer colors indicate brighter backgrounds). (*B*, *Lower*) Same traces normalized by their peaks for comparison of kinetics. Flash monitor is shown at the bottom, at time 0. The downward deflection preceding the flash is from a voltage pulse used for monitoring recording integrity. (*C*) Normalized integration time of the dim-flash response ($t_i/t_i{}^D$; *Results*) plotted against normalized background-light intensity ($I_B/I_O$). The same cells and symbols as in *A* are shown. All cells have the same data point at $t_i/t_i{}^D = 1$ and $I_B/I_O = 0$. Perforated-patch, voltage-clamp recordings (–80 mV; 23 °C) were obtained in Ames medium with fast-synaptic transmission blocked (*Materials and Methods*).

the value with no background light) was plotted against normalized background-light intensity ($I_B/I_O$), the relation again resembled that for cones (31) (Fig. 2*C* and Fig. S2 *B* and *D*). A faster response gives less temporal summation, thus contributing to the relaxation of the ipRGC's steady-light response from a transient peak to a lower plateau level (albeit only mildly compared with the contribution from the attenuation of the single-photon-response amplitude).

**Adaptation in Spike Activity of IpRGCs.** To translate the receptor-current adaptation into signals sent to the brain, we examined the ipRGC's firing activity with noninvasive, loose-patch recording from the soma (24) (*Materials and Methods*). A dim-light step produced a steady increase in firing (Fig. 3 *A* and *B*, with expanded time scale shown on right). Brighter steps produced higher initial firing rates that nonetheless relaxed to lower rates (Fig. 3 *A* and *B*). At still higher intensities, the firing rate exhibited a more complex pattern consisting of a transient peak, then a trough, sometimes a second peak, and finally a lower steady value (Fig. 3*B*, lower four traces). The spiking profile at high intensities is reminiscent of a depolarization block commonly seen in excitable cells, where a large excitation overwhelms voltage-gated ion channels to suppress or eliminate prolonged spike firing (8, 23, 24). Consequently, the transient-peak firing rate rose monotonically only for the initial $10^2$- or $10^3$-fold increase in steady-light intensity, decreasing thereafter with brighter lights (Fig. 3*B*), making it an ambiguous indicator of light intensity (Fig. 3*C*, *Upper*). On the other hand, the steady-state firing rate increased monotonically over a larger ($\sim 10^4$-fold) range in light intensity (Fig. 3*C*, *Lower*). These findings were made at 23 °C (three cells), but the same was observed at 35 °C (seven cells; Fig. S3). Because typical ipRGC-driven visual functions [e.g., pupillary constriction (32) and circadian photoreception (33)] generally respond to light beyond many seconds, the steady-state firing is presumably more relevant to the organism. In the brightest light, even the steady-state firing rate declines (Fig. 3*C*, *Lower*), rendering the M1 ipRGCs unable to signal faithfully beyond $\sim 10^9$ photons per square micron per second [roughly comparable to direct sunlight (28)]. Under in vivo conditions, the dynamic range of signaling may shift to higher or lower light intensities, depending on the balance between inhibition and excitation from the retinal circuitry (19, 34–36).

To see whether the underlying receptor current dictates the firing pattern of an ipRGC in bright steady light, we compared, with perforated-patch recording, the voltage response recorded from a cell under current-clamp to the receptor current subsequently recorded under voltage-clamp. Under current-clamp, a step of bright light typically elicited a depolarization so large that firing ceased after only a handful of spikes, followed by a relaxation of the depolarization (light adaptation) and a resumption of firing (Fig. 3*D*, *Upper* and *Inset*). This overall response profile paralleled the receptor current subsequently recorded from the same cell under voltage-clamp (Fig. 3*D*, *Lower*, and two other cells), including the second phase of depolarization being coincident with the secondary increase in the inward photocurrent. Thus, adaptation in ipRGCs appeared to originate mostly from the phototransduction mechanism rather than from voltage-gated currents (see also refs. 8, 23, and 24). With bright-enough light, even adaptation was unable to relieve the depolarization block and sustain steady firing for many cells (Fig. 3*E*).

In any case, the general inability of an ipRGC to signal for more than several log units of light intensities, as demonstrated here, may explain why multiple ipRGC subtypes exist with different sensitivities and different sustained firing rates (8, 10–12, 15), to allow signaling over a broader range of light intensity.

**Involvement of $Ca^{2+}$ Influx in Active Light Adaptation.** What mechanism underlies the active light adaptation? In rods and cones, active adaptation to background light is mediated by negative feedback triggered by a change in $Ca^{2+}$ influx (20, 37). To check for a role of $Ca^{2+}$ in adaptation by ipRGCs, we replaced all extracellular $Ca^{2+}$ with $Mg^{2+}$ (plus 1 mM EGTA to chelate $Ca^{2+}$ rapidly) by using bath-solution exchange or local perfusion

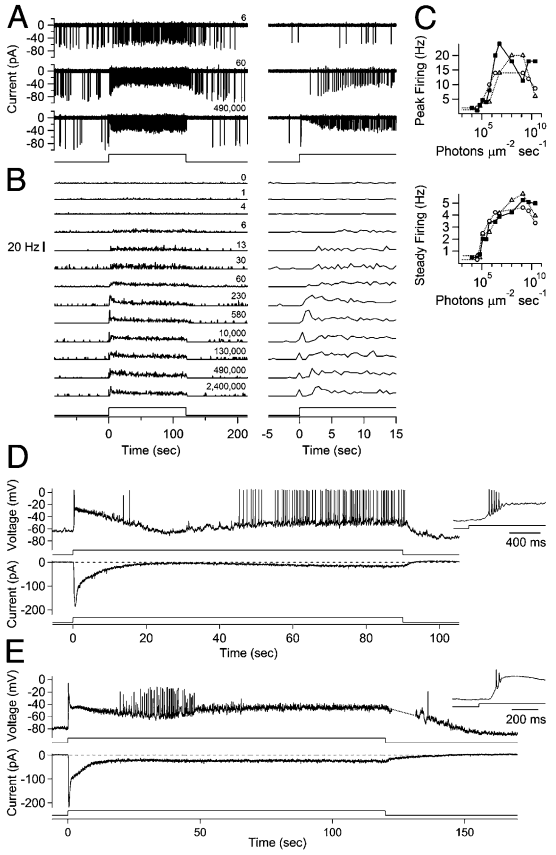


**Fig. 3.** Spiking of ipRGCs during light steps. Currents associated with spikes were recorded in loose-patch configuration ($V_{hold}$ = 0 mV; Hepes-buffered Ames pipette solution). (*A*, *Left*) Sample traces from an ipRGC, with increasing light intensity from top to bottom (diffuse, 480-nm or white expressed as equivalent 480 nm, ranging from $9.9 \times 10^3$ to $2.4 \times 10^{10}$ photons per square micron per second). The light monitor is shown at the bottom, with relative intensities marked on the right. (*A*, *Right*) Same traces shown on an expanded time base at light onset. (*B*, *Left*) Peristimulus time histograms (PSTHs) of spike activity for the same cell as in *A*, with relative intensity increasing from top to bottom. PSTHs are derived from single or multiple sweeps, with a bin width of 500 ms. (*B*, *Right*) The same PSTHs shown on an expanded time base at light onset. Light monitor trace has not been binned and, therefore, appears to rise after the increase in spike rate. (*C*) Plots of peak (*Left*) and steady (*Right*) firing rates versus light-step intensity. The cell from *A* and *B* is shown by filled squares; other cells are shown by open symbols. Peak rate is measured at the first transient peak of the PSTH or at maximum if there is no peak. The steady rate was averaged over several seconds at the end of the light step. Note the region of negative slope at high intensities. (*D*) Perforated-patch recordings from one cell, first in current-clamp (no injected current) (*Upper*), and then in voltage clamp (–80 mV) (*Lower*), in response to the same step of light delivering $1.5 \times 10^9$ photons per square micron per second (480 nm; diffuse). Note that the photocurrent is large enough to produce depolarization block (highlighted in *Inset*). Transient depolarization block is especially prolonged for this cell, although periods of suppressed spiking approaching 20 s also have been observed in loose-patch recording. (*E*) Same experiment on another cell, where even the steady current eventually blocked spiking. The break in trace (dotted line) is attributable to the limited acquisition sweep length, with true duration shown. *Inset* shows response at light onset. The step was diffuse, white light delivering the equivalent of $3.3 \times 10^{10}$ photons per square micron per second at 480 nm. In *A*–*E*, recordings were from flat-mount retina at 23 °C, in Ames medium with fast-synaptic transmission blocked (*Materials and Methods*). Similar results were observed at 35 °C for *A*–*C* (Fig. S3).

of the soma (with both giving similar results, from three and four cells, respectively). A dim flash (spot of 40–100 μm in diameter centered on the soma) in 0-$Ca^{2+}$ solution elicited a response that had an initial rising phase no different from control, but its time to peak, $t_p$, was delayed; thus, the transient-peak amplitude became larger (Fig. 4 *A* and *B*). From collected data, $t_p$ increased in 0-$Ca^{2+}$ to 1.34 ± 0.19-fold, and the transient-peak amplitude increased to 4.0 ± 1.9-fold (seven cells; Fig. 4*C*). The 0-$Ca^{2+}$ effect was largely reversible (Fig. 4 *A*–*C*). A similar $Ca^{2+}$ effect was observed for the bright-flash response (Fig. 4*D*), although with a smaller fractional increase in peak photocurrent (2.0 ± 0.4-fold; four cells). We found a similar effect for dissociated ipRGCs (1.7 ± 0.4-fold increase in peak current for bright flashes; three cells; no EGTA; Fig. S4). Finally, removing external $Ca^{2+}$ without replacement with $Mg^{2+}$ gave the same overall result, as did replacing both $Ca^{2+}$ and $Mg^{2+}$ with $Ba^{2+}$ (two cells and one cell, respectively). Generally, $Mg^{2+}$ and $Ba^{2+}$ lack the intracellular effects of $Ca^{2+}$ (38). Thus, $Ca^{2+}$ appears to enter the cell during the light response to initiate adaptation by accelerating the termination of phototransduction. Because our voltage-clamp experiments were performed at −80 mV (thus with voltage-gated Ca channels in the closed state), and ipRGC phototransduction appears independent of intracellular $Ca^{2+}$ stores (39, 40), the $Ca^{2+}$ likely enters through the phototransduction channel, which consists of at least the transient receptor potential canonical (TRPC) channel isoforms 6 and 7 (i.e., TRPC6 and TRPC7) (28, 40–42). In physiological conditions, additional negative feedback may be mediated by $Ca^{2+}$ entry through voltage-gated Ca channels (39). Interestingly, the degrees of modulation of the ipRGC's dim-flash response in amplitude and time course by $Ca^{2+}$ feedback, as observed here, are quite similar to those found in rods and cones (43).

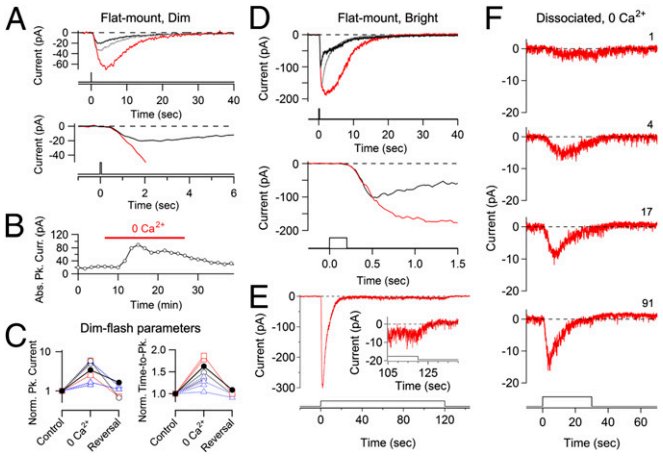


**Fig. 4.** Calcium-dependent negative feedback in melanopsin phototransduction. A perforated-patch, voltage-clamp recording was obtained at −80 mV in the flat-mount retina. (*A*, *Upper*) Dim-flash response from an ipRGC first in control solution (black) and then with extracellular $Ca^{2+}$ replaced by $Mg^{2+}$ and EGTA (red), followed by return to control solution (gray) with bath exchange. (*A*, *Bottom*) Detail of the rising phase of the response. Flash intensity was $9.3 \times 10^5$ photons per square micron (480 nm), with a 100-μm spot centered on soma. The light monitor is shown at the bottom. (*B*) Normalized peak amplitude of the dim-flash response plotted against time for the experiment in *A*. (*C*) Data collected from many cells, recorded in the flat-mount retina, of the 0-$Ca^{2+}$ effect on the peak amplitude (*Left*) and time to peak (*Right*) for dim-flash responses, with (*i*) $Ca^{2+}$ replaced by $Mg^{2+}$ and EGTA with bath exchange (black open circles); (*ii*) $Ca^{2+}$ removed without $Mg^{2+}$ substitution, plus EGTA with bath exchange (red open squares); or (*iii*) as in the first condition (*i*) but with local perfusion of the recorded cell (blue open triangles). Filled symbols are for the cell in *A* and *B*. Photocurrents in the control solution were verified to be in the linear range. Dim-flash stimuli (480 nm) were used, delivered in a 40- to 100-μm spot centered on the soma. (*D*, *Upper*) Response of another ipRGC to a near-saturating flash in control solution (black), after bath substitution of $Ca^{2+}$ by $Mg^{2+}$ and EGTA (red) and following return to control solution (gray). (*D*, *Lower*) Detail of the rising phase of the responses in control and 0 $Ca^{2+}$. Flash intensity was $7.9 \times 10^9$ photons per square micron (white light expressed as equivalent 480-nm photons), with a 100-μm spot centered on soma. The light monitor is shown at the bottom. No overall time course of the experiment as in *B* is shown here because part of the $Ca^{2+}$ exchange was done during other stimuli. (*E*) Strong adaptation still exists in 0 $Ca^{2+}$, as revealed by a light step (expanded axes in *Inset* to show the response's steady phase). Stimulus was a 40-μm spot of white light, centered on the soma, delivering the equivalent of $3.9 \times 10^{10}$ photons per square micron per second of 480-nm light. (*F*) Same phenomenon of adaptation in 0 $Ca^{2+}$ shown by a dissociated cell. Relative light intensity (480-nm diffuse light, 30-s step) increasing from top to bottom, with absolute values from $4.3 \times 10^4$ to $3.9 \times 10^6$ photons per square micron per second. Stimuli for this cell were delivered rapidly (every 2 min) to reduce the impact of rundown in 0 $Ca^{2+}$; as a result, the light response may be faster and smaller than expected because of cumulative adaptation; 10 μM 9-*cis* retinal was continuously present in the bath solution for this cell. For *A*–*F*, recordings were at 23 °C, and fast-synaptic transmission was blocked in the case of flat-mount preparation.

**$Ca^{2+}$-Independent Adaptation.** To see whether adaptation exists in the absence of $Ca^{2+}$ influx, we turned to a light step for stimulation. Even in the absence of external $Ca^{2+}$ (replaced by $Mg^{2+}$ and 1 mM EGTA), an in situ ipRGC's response to a bright light step still showed prominent relaxation, indicating strong adaptation, albeit slower than in normal-$Ca^{2+}$ solution (Fig. 4*E*; four cells). The same was found for acutely dissociated ipRGCs under the same treatment (Fig. 4*F*; three cells). In Fig. 4*F*, second trace from top, where adaptation is already prominent, the rate of melanopsin activation is only ∼0.4 molecules $sec^{-1}$ (legend and *SI Text*). Thus, adaptation occurs although melanopsin depletion is negligible, implicating the existence of $Ca^{2+}$-independent, active adaptation. No obvious $Ca^{2+}$-independent, active adaptation has been reported in rods and cones (20, 37) (especially so in situ) or in invertebrate rhabdomeric photoreceptors (44, 45).

## Discussion

Previously, we have found (24) that M1 ipRGCs, like rods and cones (20), show a flash intensity–response relation that can be described approximately by the Michaelis equation. We now find that the receptor current of M1 ipRGCs adapts to background light in a manner also quantitatively similar to that shown by rods and cones, namely, according to the Weber–Fechner law. There is no simple mathematical connection between the Michaelis behavior and the Weber–Fechner law. Both equations are phenomenological descriptions of a complex process, giving no direct clue to the underlying mechanism. The flash intensity–response relation, measured at the transient peak of the flash responses, reflects the effect of light adaptation that is in progress but still incomplete at response peak. The Weber–Fechner law, on the other hand, reflects adaptation that has already reached steady state at a given light-step intensity; it roughly corresponds to the slope of the steady-state step intensity–response relation [which, incidentally, is much shallower than the flash intensity–response relation (26)]. Because a common underlying adaptation process ultimately dictates both the flash and the step intensity–response relations, it is perhaps not surprising that, given the same Michaelis behavior by rods/cones and the ipRGCs, both cell types might also show the Weber–Fechner behavior. Still, rods/cones and ipRGCs have distinct phototransduction mechanisms, with the former involving a cGMP-mediated signaling pathway (20) and the latter a phospholipase-C-mediated pathway (28, 40–42). The cellular mechanism underlying light adaptation in rods and cones is now known to be elaborate, with consequences that happen to be describable (approximately) by the simple mathematical forms of the Michaelis and the Weber–Fechner relations. The mechanism underlying light adaptation in ipRGCs is likely as complex and is only beginning to be understood (46, 47). From

this standpoint, it is remarkable that the same equations are still able to capture its essence.

As mentioned in the introductory paragraphs, Weber–Fechner adaptation confers to rod- and cone-based vision the perception of contrast more so than brightness, promoting a constant object appearance over a ~10-log-unit range in ambient light level (21). This important property in image vision is preserved along the visual pathway to the level of consciousness. For nonimage vision, although adaptation is certainly beneficial for increasing the signaling dynamic range, the exact implication of Weber–Fechner behavior is less obvious. Because ipRGCs are now known to also contribute to conscious vision (12, 48–52), this adaptation behavior may have more to do with the latter function. It would, thus, be useful to know whether the other ipRGC subtypes [which supposedly are more involved in image vision compared with M1 cells (12, 15)] show similar adaptation behavior. This will not be an easy endeavor, however, because of their much smaller photocurrents and lower sensitivities. At the same time, exactly how the Weber–Fechner behavior at the receptor-current level is encoded at the level of spike firing in the ipRGC axons and beyond is also unclear at present.

The ipRGC-driven component of the in vivo light responses recorded in the suprachiasmatic and other hypothalamic nuclei (53) typically display little relaxation in firing after light onset but, nonetheless, have firing rates throughout of no more than a few Hz, rather comparable to the adapted, steady rates found by us here for ipRGCs. Thus, the adapted, sustained photocurrent and its associated firing in ipRGCs may indeed be more relevant to behavior, with the transient-peak components perhaps filtered out during transmission [for example, at axonal branch points (54) or at the synapse] to postsynaptic cells.

Finally, the mechanistic details of the $Ca^{2+}$-dependent and $Ca^{2+}$-independent adaptations remain unknown. At least for the brightest stimuli, part of the $Ca^{2+}$-independent adaptation may reflect the very low level of melanopsin in ipRGCs such that the depletion of signaling melanopsin becomes significant. Although melanopsin is reported to be bistable (4, 6, 55–57), whether this bistability is absolute and how quickly melanopsin returns to the signaling state are still unclear at present.

## Materials and Methods

**Tissue Preparation.** All procedures were approved by the Institutional Animal Care and Use Committee of The Johns Hopkins University School of Medicine. BAC transgenic mice (P20-90) with ipRGCs labeled by tdTomato were used (24). Mice were dark-adapted overnight, and dissections performed in dim-red light. An animal was anesthetized, enucleated, and euthanized. An eye was hemisected, the retina was teased free, and vitreous was removed with forceps. For flat-mount recording, the retina was flattened with cuts and held in the recording chamber, photoreceptors down, by a platinum-iridium frame strung with nylon fibers. For dissociation, the retina was subdivided and exposed for 30 min at 35 °C to an "ionic Ames" solution (see below) containing 0.25–1 mg/mL Protease XXIII (Sigma-Aldrich) and 50 U/mL collagenase IV (Worthington). The pieces were rinsed with ionic Ames, transferred to the same solution containing 1 mg/mL BSA and 1 mg/mL trypsin inhibitor at 23 °C, and kept for 8–12 h until use. As needed, tissue pieces were transferred into a dissociation solution and triturated to disperse cells. The dissociation solution contained the following (in mM): 70 $Na_2SO_4$, 2 $K_2SO_4$, 5 $MgSO_4$, 0–3 $CaCl_2$, 10 Hepes, 10 glucose, and 60 sucrose (pH 7.4 with NaOH). DNase (0.05%; Worthington) was sometimes added to reduce cell clumping following trituration.

**Electrophysiology.** Bicarbonate-buffered Ames (containing synaptic blockers for flat-mount experiments) was equilibrated with 95% $O_2$/5% $CO_2$ (vol/vol) and run at ~5 mL/min through a 1-mL chamber. Temperature was controlled with an in-line heater and monitored by a thermistor in the chamber. IpRGCs were visualized using a few seconds of fluorescence light, followed by infrared differential interference contrast microscopy. For the flat-mount retina, the inner limiting membrane overlying ipRGCs was locally removed with a pipette before recording.

Pipettes were 2–5 MΩ in resistance and wrapped with parafilm to reduce capacitance. Perforated-patch recordings were with a KCl-based pipette solution (see below) containing 125–250 μM amphotericin B. No voltage-clamp experiments on steady photocurrents were done at above room temperature because of fragility of perforated-patch recordings. For loose-patch recordings, the pipette contained Hepes-buffered Ames (see below). An Axopatch 200B or Multiclamp 700B in voltage-clamp or current-clamp mode was used. Recording stability was checked periodically with a dim test flash, and series resistance was monitored. Liquid-junction potential was corrected. Photocurrent was low-pass–filtered at 2 Hz (dim flashes) or 10 Hz (bright flashes) and membrane voltage at 10 kHz. Loose-patch recording bandwidth was 10 Hz to 1 kHz. Sampling exceeded the Nyquist minimum.

For perforated-patch recordings, the series resistance was typically ~50 MΩ, although higher resistances were tolerated because they were less frequently associated with spontaneous breakthroughs. Because the photocurrent is very sensitive to dialysis, its stability was used as a monitor of the integrity of the perforated-patch recording. Loose-patch recordings of action currents were made in voltage-clamp mode ($V_{command}$ = 0 mV).

Space-clamp concerns were reduced by the slowness of the photocurrent typically measured (time scale of seconds), the flatness of the current–voltage relation for >10 mV on either side of the holding voltage of –80 mV (22), the high input resistance of the neurons (~1 GΩ typical) and, often, by the stimulus being a small (40–100 μm) light spot centered on the in situ soma, and by the inclusion of tetrodotoxin in the extracellular solution (except when spikes were studied). Although these considerations do not guarantee adequate space clamp, the dim-flash and single-photon responses were indistinguishable whether recorded from a dissociated cell or from an in situ cell stimulated at the soma or 100 μm away at the dendrites (24).

Infrared illumination was attenuated or turned off during recording, except for intermittent monitoring of the cell or pipette position. The Faraday cage was light-proof.

Data were analyzed with custom routines written in Igor Pro (Wavemetrics) and presented as means ± SD.

**Solutions.** The intracellular solution for perforated-patch recordings was as follows (in mM): 110 KCl, 13 NaCl, 2 $MgCl_2$, 1 $CaCl_2$, 10 EGTA, and 10 Hepes (pH 7.2 with KOH). Many other anions have been tested, but $Cl^-$ gave the lowest and most stable series resistances. Amphotericin B was dissolved in DMSO to make 100× aliquots and stored in the dark at –20 °C for <2 wk. Amphotericin-containing internal solution was sonicated before loading into each patch-pipette. A liquid-junction potential of +3 mV has been corrected. For loose-patch recordings, pipettes were filled with a Hepes-buffered ionic Ames solution (in mM): 140 NaCl, 3.1 KCl, 0.5 $KH_2PO_4$, 1.5 $CaCl_2$, 1.2 $MgSO_4$, 6 glucose, and 10 Hepes (pH 7.4 with NaOH). Ionic Ames is formulated with ion concentrations similar to those in Ames but without other supplements.

The extracellular solution was bicarbonate-buffered Ames medium, or ionic Ames medium (in mM): 120 NaCl, 22.6 $NaHCO_3$, 3.1 KCl, 0.5 $KH_2PO_4$, 1.5 $CaCl_2$, 1.2 $MgSO_4$, and 6 glucose, equilibrated with 95% $O_2$/5% $CO_2$. Fast-synaptic transmission was blocked by adding to the external solution (in mM): 3 kynurenate and 0.1 picrotoxin. Often, 100 μM DL-2-amino-4-phosphonobutyric acid, 10 μM strychnine, and 200–300 nM TTX were also added; 10 μM 9-*cis* retinal was added to some experiments on dissociated cells to increase photosensitivity (24).

For $Ca^{2+}$ removal, $CaCl_2$ was either replaced by 2.9 mM $MgCl_2$ or simply removed without replacement plus 1 mM EGTA added. With dissociated cells, flash experiments consisted of $CaCl_2$ being simply replaced with equimolar $MgCl_2$, whereas light-step experiments had $CaCl_2$ replaced by 2.9 mM $MgCl_2$ and 1 mM EGTA. In experiments involving $Ba^{2+}$, $CaCl_2$ and $MgCl_2$ were together replaced by 3.7 mM $BaCl_2$ and 1 mM EGTA. Concentrations were chosen to maintain the same divalent activity across conditions, as calculated by MaxChelator (http://maxchelator.stanford.edu). Local perfusion was performed with a capillary (~200-μm diameter) positioned next to the ipRGC soma.

External $Ca^{2+}$ does not appear to play a substantial role in the early rising phase of the light response (*Results*). However, continuous exposure to 0 $Ca^{2+}$ causes gradual rundown of the photocurrent, possibly reflecting cell-condition decline (41), and explains the smaller steady response observed in 0 $Ca^{2+}$ (Fig. 4*E*). The strategy of avoiding this rundown by rapidly switching between $Ca^{2+}$-containing and $Ca^{2+}$-free solutions is impractical because the adaptation time course of the ipRGC's step response is not well resolved from that of rundown and because of the fragility of perforated-patch recording.

**Light Stimulation.** The principal light source was a 75-W xenon arc lamp, modulated by a heat filter, calibrated neutral-density filters, and 10-nm bandpass filters. The beam was controlled by an electronic shutter and delivered to the microscope via a light guide. Flashes were 10–200 ms in

duration, and steps were 1–3 min long. The secondary source, specifically for flashes, was a pair of xenon flash lamps (Rapp OptoElectronic) with outputs combined and routed to the microscope via a bifurcated light guide. Neutral-density and 10-nm band-pass filters controlled intensity and wavelength, respectively, and flashes were ~1 ms in duration. Light was passed through an iris to control the spot size (centered on the soma, with a diameter at the preparation of 40 μm with the iris fully constricted and 730 μm with iris wide open; the latter is designated as "diffuse light"), reflected off a cold mirror to further minimize heat, and focused onto the cell as epi-illumination through the 40× objective.

Flashes were temporally spaced to allow full recovery between presentations (typically 30–120 s, depending on intensity). Unless otherwise noted, light steps were followed by dim test flashes to ensure full recovery before the next step, and the recording was terminated if the final recovery was incomplete. White flashes were converted to equivalent 480-nm flashes by response matching (24). We used flashes that are "impulse" stimuli; that is, light intensity and duration are proportionally interchangeable without affecting the response. The light intensity was periodically calibrated with a radiometer.

**ACKNOWLEDGMENTS.** We thank Donggen Luo, Zheng Jiang, Chih-Chun Lin, Wendy Yue, Lihui Cao, and Tian Xue of the K.-W.Y. laboratory and Alan Emanuel of the M.T.H.D. laboratory for providing comments on the manuscript. This work was supported by National Institutes of Health Grant EY14596, an António Champalimaud Vision Award (Portugal) (to K.-W.Y), and a National Research Service Award (to M.T.H.D.).

1. Rollag MD, Berson DM, Provencio I (2003) Melanopsin, ganglion-cell photoreceptors, and mammalian photoentrainment. *J Biol Rhythms* 18(3):227–234.
2. Hankins MW, Peirson SN, Foster RG (2008) Melanopsin: An exciting photopigment. *Trends Neurosci* 31(1):27–36.
3. Bailes HJ, Lucas RJ (2010) Melanopsin and inner retinal photoreception. *Cell Mol Life Sci* 67(1):99–111.
4. Do MTH, Yau K-W (2010) Intrinsically photosensitive retinal ganglion cells. *Physiol Rev* 90(4):1547–1581.
5. Hatori M, Panda S (2010) The emerging roles of melanopsin in behavioral adaptation to light. *Trends Mol Med* 16(10):435–446.
6. Schmidt TM, Chen SK, Hattar S (2011) Intrinsically photosensitive retinal ganglion cells: Many subtypes, diverse functions. *Trends Neurosci* 34(11):572–580.
7. Sand A, Schmidt TM, Kofuji P (2012) Diverse types of ganglion cell photoreceptors in the mammalian retina. *Prog Retin Eye Res* 31(4):287–302.
8. Schmidt TM, Kofuji P (2009) Functional and morphological differences among intrinsically photosensitive retinal ganglion cells. *J Neurosci* 29(2):476–482.
9. Berson DM, Castrucci AM, Provencio I (2010) Morphology and mosaics of melanopsin-expressing retinal ganglion cell types in mice. *J Comp Neurol* 518(13):2405–2422.
10. Schmidt TM, Kofuji P (2011) Structure and function of bistratified intrinsically photosensitive retinal ganglion cells in the mouse. *J Comp Neurol* 519(8):1492–1504.
11. Tu DC, et al. (2005) Physiologic diversity and development of intrinsically photosensitive retinal ganglion cells. *Neuron* 48(6):987–999.
12. Ecker JL, et al. (2010) Melanopsin-expressing retinal ganglion-cell photoreceptors: Cellular diversity and role in pattern vision. *Neuron* 67(1):49–60.
13. Jain V, Ravindran E, Dhingra NK (2012) Differential expression of Brn3 transcription factors in intrinsically photosensitive retinal ganglion cells in mouse. *J Comp Neurol* 520(4):742–755.
14. Baver SB, Pickard GE, Sollars PJ, Pickard GE (2008) Two types of melanopsin retinal ganglion cell differentially innervate the hypothalamic suprachiasmatic nucleus and the olivary pretectal nucleus. *Eur J Neurosci* 27(7):1763–1770.
15. Estevez ME, et al. (2012) Form and function of the M4 cell, an intrinsically photosensitive retinal ganglion cell type contributing to geniculocortical vision. *J Neurosci* 32(39):13608–13620.
16. Gooley JJ, Lu J, Fischer D, Saper CB (2003) A broad role for melanopsin in nonvisual photoreception. *J Neurosci* 23(18):7093–7106.
17. Hattar S, et al. (2006) Central projections of melanopsin-expressing retinal ganglion cells in the mouse. *J Comp Neurol* 497(3):326–349.
18. Hattar S, Liao HW, Takao M, Berson DM, Yau KW (2002) Melanopsin-containing retinal ganglion cells: Architecture, projections, and intrinsic photosensitivity. *Science* 295(5557):1065–1070.
19. Dacey DM, et al. (2005) Melanopsin-expressing ganglion cells in primate retina signal colour and irradiance and project to the LGN. *Nature* 433(7027):749–754.
20. Luo D-G, Kefalov V, Yau K-W (2008) Phototransduction in rods and cones. *The Senses: A Comprehensive Reference*, eds Masland R, Albright TD (Academic Press, Oxford), Vol 1, pp 269–301.
21. Shapley R, Enroth-Cugell C (1984) Visual adaptation and retinal gain controls. *Prog Retinal Res* 3:263–346.
22. Warren EJ, Allen CN, Brown RL, Robinson DW (2003) Intrinsic light responses of retinal ganglion cells projecting to the circadian system. *Eur J Neurosci* 17(9):1727–1735.
23. Wong KY, Dunn FA, Berson DM (2005) Photoreceptor adaptation in intrinsically photosensitive retinal ganglion cells. *Neuron* 48(6):1001–1010.
24. Do MTH, et al. (2009) Photon capture and signalling by melanopsin retinal ganglion cells. *Nature* 457(7227):281–287.
25. Tamura T, Nakatani K, Yau K-W (1989) Light adaptation in cat retinal rods. *Science* 245(4919):755–758.
26. Nakatani K, Tamura T, Yau K-W (1991) Light adaptation in retinal rods of the rabbit and two other nonprimate mammals. *J Gen Physiol* 97(3):413–435.
27. Nakatani K, Yau K-W (1988) Calcium and light adaptation in retinal rods and cones. *Nature* 334(6177):69–71.
28. Xue T, et al. (2011) Melanopsin signalling in mammalian iris and retina. *Nature* 479(7371):67–73.
29. Chen SK, Badea TC, Hattar S (2011) Photoentrainment and pupillary light reflex are mediated by distinct populations of ipRGCs. *Nature* 476(7358):92–95.
30. Schnapf JL, Nunn BJ, Meister M, Baylor DA (1990) Visual transduction in cones of the monkey *Macaca fascicularis*. *J Physiol* 427:681–713.
31. Matthews HR, Fain GL, Murphy RL, Lamb TD (1990) Light adaptation in cone photoreceptors of the salamander: A role for cytoplasmic calcium. *J Physiol* 420:447–469.
32. Gamlin PD, et al. (2007) Human and macaque pupil responses driven by melanopsin-containing retinal ganglion cells. *Vision Res* 47(7):946–954.
33. Nelson DE, Takahashi JS (1991) Sensitivity and integration in a visual pathway for circadian entrainment in the hamster (Mesocricetus auratus). *J Physiol* 439:115–145.
34. Wong KY, Dunn FA, Graham DM, Berson DM (2007) Synaptic influences on rat ganglion-cell photoreceptors. *J Physiol* 582(Pt 1):279–296.
35. Schmidt TM, Kofuji P (2010) Differential cone pathway influence on intrinsically photosensitive retinal ganglion cell subtypes. *J Neurosci* 30(48):16262–16271.
36. Perez-Leon JA, Warren EJ, Allen CN, Robinson DW, Brown RL (2006) Synaptic inputs to retinal ganglion cells that set the circadian clock. *Eur J Neurosci* 24(4):1117–1123.
37. Fain GL (2011) Adaptation of mammalian photoreceptors to background light: Putative role for direct modulation of phosphodiesterase. *Mol Neurobiol* 44(3):374–382.
38. Hille B (2001) *Ion Channels of Excitable Membranes* (Sinauer Associates, Sunderland, MA).
39. Hartwick AT, et al. (2007) Light-evoked calcium responses of isolated melanopsin-expressing retinal ganglion cells. *J Neurosci* 27(49):13468–13480.
40. Sekaran S, et al. (2007) 2-Aminoethoxydiphenylborane is an acute inhibitor of directly photosensitive retinal ganglion cell activity in vitro and in vivo. *J Neurosci* 27(15):3981–3986.
41. Graham DM, et al. (2008) Melanopsin ganglion cells use a membrane-associated rhabdomeric phototransduction cascade. *J Neurophysiol* 99(5):2522–2532.
42. Perez-Leighton CE, Schmidt TM, Abramowitz J, Birnbaumer L, Kofuji P (2011) Intrinsic phototransduction persists in melanopsin-expressing ganglion cells lacking diacylglycerol-sensitive TRPC subunits. *Eur J Neurosci* 33(5):856–867.
43. Nakatani K, Yau K-W (1989) Sodium-dependent calcium extrusion and sensitivity regulation in retinal cones of the salamander. *J Physiol* 409:525–548.
44. Hardie RC, Postma M (2008) Phototransduction in microvollar photoreceptors of Drosophila and other invertebrates. *The Senses: A Comprehensive Reference*, eds Masland R, Albright TD (Academic Press, Oxford), Vol 1, pp 77–130.
45. Payne R, Wang Y (2010) Phototransduction in Limulus photoreceptors. *Encylopedia of the Eye*, ed Dartt DA (Academic, Oxford), Vol 3, pp 381–388.
46. Blasic JR, Jr., Brown RL, Robinson PR (2012) Phosphorylation of mouse melanopsin by protein kinase A. *PLoS ONE* 7(9):e45387.
47. Blasic JR, Jr., Lane Brown R, Robinson PR (2012) Light-dependent phosphorylation of the carboxy tail of mouse melanopsin. *Cell Mol Life Sci* 69(9):1551–1562.
48. Brown TM, et al. (2010) Melanopsin contributions to irradiance coding in the thalamo-cortical visual system. *PLoS Biol* 8(12):e1000558.
49. Zaidi FH, et al. (2007) Short-wavelength light sensitivity of circadian, pupillary, and visual awareness in humans lacking an outer retina. *Curr Biol* 17(24):2122–2128.
50. Johnson J, et al. (2010) Melanopsin-dependent light avoidance in neonatal mice. *Proc Natl Acad Sci USA* 107(40):17374–17378.
51. Brown TM, et al. (2012) Melanopsin-based brightness discrimination in mice and humans. *Curr Biol* 22(12):1134–1141.
52. Horiguchi H, Winawer J, Dougherty RF, Wandell BA (2013) Human trichromacy revisited. *Proc Natl Acad Sci USA* 110(3):E260–E269.
53. Brown TM, Wynne J, Piggins HD, Lucas RJ (2011) Multiple hypothalamic cell populations encoding distinct visual information. *J Physiol* 589(Pt 5):1173–1194.
54. Yau K-W (1976) Receptive fields, geometry and conduction block of sensory neurones in the central nervous system of the leech. *J Physiol* 263(3):513–538.
55. Sexton TJ, Golczak M, Palczewski K, Van Gelder RN (2012) Melanopsin is highly resistant to light and chemical bleaching in vivo. *J Biol Chem* 287(25):20888–20897.
56. Matsuyama T, Yamashita T, Imamoto Y, Shichida Y (2012) Photochemical properties of mammalian melanopsin. *Biochemistry* 51(27):5454–5462.
57. Brown TM, et al. (2013) The melanopic sensitivity function accounts for melanopsin-driven responses in mice under diverse lighting conditions. *PLoS ONE* 8(1):e53583.